This document is a preprint of: R. Bomfin, A. Nimr and G. Fettweis, "A Study on Iterative Equalization for DFTs-OFDM Waveform under sub-THz Channels," in Proceedings of 2022 IEEE 19th Annual Consumer Communications Networking Conference (CCNC 2022), Virtual Conference, (pp. 1-6), Jan 2022. DOI:10.1109/CCNC49033.2022.9700594

A Study on Iterative Equalization for DFTs-OFDM Waveform under sub-THz Channels

Roberto Bomfin, Ahmad Nimr and Gerhard Fettweis, *Fellow, IEEE*
Vodafone Chair Mobile Communication Systems, Technische Universität Dresden, Germany
roberto.bomfin@ifn.et.tu-dresden.de, ahmad.nimr@ifn.et.tu-dresden.de and gerhard.fettweis@tu-dresden.de

***Abstract*—Sub-THz communications have been recently considered as an alternative to increase the data rate for the 6th generation (6G) of mobile systems. Since maintaining a reasonable link budget becomes more difficult in higher frequencies, the DFTs-OFDM waveform has been considered as a candidate for sub-THz transmissions, because it has low power-to-average peak ratio (PAPR) in comparison to waveforms with higher PAPR, e.g., orthogonal frequency division multiplexing (OFDM). Additionally, recent channel measurements at $140\,\mathrm{GHz}$ have demonstrated that the channel is frequency-selective. This fact motivated us to investigate the DFTs-OFDM link-level performance under an empirical sub-THz channel with the employment of an iterative receiver, since it is known that iterative equalization can mitigate the effects of inter-symbol interference. For this purpose, we consider the minimum mean squared error with parallel interference cancellation (MMSE-PIC) iterative receiver, with convolutional and low-density parity-check (LDPC) codes. The results show that for medium frequency selectivity, LDPC codes provide best performance in terms of frame error rate, but for high selectivity, the convolutional code system has the best performance.**

***Index Terms*—sub-THz, DFTs-OFDM, MMSE-PIC, LDPC code, convolutional code**

I. Introduction

THE industry and research communities have recently started the research on the 6th generation (6G) of mobile networks [1]–[4]. Due to large spans of available spectrum on the order of several GHz, sub-THz communication have been considered an important aspect of 6G [5]. However, there are several challenges to be faced in this frequency range. Keeping a good link budget is more challenging as the frequency increases, because maintaining the same link budget as the transmission for the same transmit requires more directive antennas. Building such antennas is challenging, especially with mobility where beam tracking is needed. Thus, it is necessary to use the transmit power as efficient as possible. For this reason, one of the considered waveforms for 6G is the discrete Fourier transform-spread OFDM (DFTs-OFDM) due to its low peak-to-average power ratio (PAPR) [6] and simple equalization in the frequency domain.

In this paper, we utilize an empirical sub-THz channel model based on the measurements from Aalto Univeristy, Finland, presented in [7], [8], where power angular delay profile (PADP) measurements have been collected from different transmitter and receiver positions in a shopping mall in Finland. The measurements reveal that in general the wireless channel at $140\,\mathrm{GHz}$ is frequency-selective due to the time dispersion. Since this type of channel causes inter-symbol interference (ISI) on the DFTs-OFDM waveform, we are motivated to investigate the performance of this system at $140\,\mathrm{GHz}$ employing an iterative receiver. The idea of using an iterative receiver is to improve the system link-level performance by cancelling the interference caused by multipath. In this work, we consider the low-complexity mininmum mean squared error with parallel iterference cancellation (MMSE-PIC) receiver used in [9], which is also valid for DFT-s OFDM. The iterative equalization is carried out by exchanging extrinsic information between the equalizer and soft-input soft-output (SISO) decoder.

The contributions of this paper are given in the following. Firstly, we investigate whether iterative equalization in the $140\,\mathrm{GHz}$ can provide performance gains in relation to a regular linear equalization. Secondly, we compare the performance of two different encoders, namely, convolutional and low-density parity-check (LDPC). We consider the SISO convolutional encoder because it has been commonly used in conjunction with iterative equalization in several recent works in the literature [10]–[13]. Additionally, it is well accepted that LDPC codes are superior to convolutional codes under additive white Gaussian noise (AWGN) channels, and it has been selected in 5G new radio (NR) for long packet sizes due to its good performance and good implementation aspects [14]. In [15], it has been shown that under multiple-input multiple-output (MIMO) spatial multiplexing scenario, which is a high ISI condition due to inter antenna interference, the LDPC coding provided inferior performance than the convolutional code. In this manuscript we investigate the reliability performance of both encoders under frequency-selective channels with iterative equalization with single antenna under different ISI conditions, or equivalently, under different levels of selectivity in frequency. The results show that under a moderate frequency-selective channel, the LDPC encoder has better performance than the convolutional, whereas for the highly frequency-selective channel, the convolutional code is better.

The reminder of the paper is organized as follows; Section II presents the system model and provides an overview on the iterative receiver. Section III is dedicated to describing the channel model based on the empirical measurements at 140 GHz. The numerical results comparing convolutional and LDPC coding are presented in Section IV. Finally, Section V concludes the paper with outlook on future works.

II. System Model

A. Transmitter

At the transmitter, the bit-interleaved coded modulation (BICM) transmission [16] is considered, in which a vector of information bits $\mathbf{b} \in \{0,1\}^{N_\mathrm{b}}$ is encoded creating the coded

This document is a preprint of: R. Bomfin, A. Nimr and G. Fettweis, "A Study on Iterative Equalization for DFTs-OFDM Waveform under sub-THz Channels," in Proceedings of 2022 IEEE 19th Annual Consumer Communications Networking Conference (CCNC 2022), Virtual Conference, (pp. 1-6), Jan 2022. DOI:10.1109/CCNC49033.2022.9700594

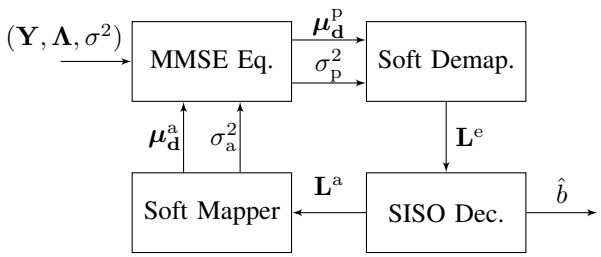

Fig. 1. Block diagram of the iterative receiver based on [9].

bit stream $\mathbf{c} = \mathrm{enc}(\mathbf{b}) \in \{0,1\}^{N_{\mathrm{c}}}$, where $R = N_{\mathrm{b}}/N_{\mathrm{c}}$ is the coding rate, with N_{b} and N_{c} are the number of uncoded and coded bits, respectively. Subsequently, the coded bits $\mathbf{c}$ are interleaved as $\mathbf{c}' = \Pi(\mathbf{c})$, where $\Pi(\cdot)$ represents the interleaver function. The interleaved coded bits $\mathbf{c}'$ are then mapped onto a QAM constellation set $\mathcal{S}$ with cardinality $|\mathcal{S}| = J$, generating the data vector $\mathbf{d} = \mathrm{mapper}(\mathbf{c}') \in \mathcal{S}^N$, with $\mathbb{E}(\mathbf{d}\mathbf{d}^{\mathrm{H}}) = E_{\mathrm{s}}\mathbf{I}$, where E_{s} is the average energy per symbol.

In this paper, we are interested in investigating the DFTs-OFDM waveform with frequency-domain processing. In this case, the QAM symbols are modulated with the DFT matrix $\mathbf{F}$[1] as

$$\mathbf{X} = \mathbf{F}^{\mathrm{H}}\mathbf{d}, \tag{1}$$

being $\mathbf{X} \in \mathbb{C}^N$ the modulated data in the frequency domain.

B. Received Signal

Under perfect time and frequency synchronization, the frequency-domain received signal $\mathbf{Y} \in \mathbb{C}^N$ is described as

$$\mathbf{Y} = \mathbf{\Lambda}\mathbf{F}^{\mathrm{H}}\mathbf{d} + \mathbf{W}, \tag{2}$$

where $\mathbf{\Lambda} \in \mathbb{C}^{N\times N}$ is the diagonal channel matrix whose elements correspond to the channel response in the frequency domain. The elements of $\mathbf{W} \sim \mathcal{CN}\left(0, \mathbf{I}_N\sigma^2\right)$ denote the AWGN samples with power σ^2.

C. Iterative Receiver

In the following, we briefly describe the iterative receiver based on the MMSE-PIC, which is depicted in Fig. 1. The processing is carried out in the frequency domain and is based on the system model of equation (2).

1) Linear Equalization: The equalizer computes the mean and error variance of the estimated data symbols as

$$\boldsymbol{\mu}_{\mathbf{d}}^{\mathrm{p}} = \boldsymbol{\mu}_{\mathbf{d}}^{\mathrm{a}} + \frac{1}{\lambda}\mathbf{F}^{\mathrm{H}}\mathbf{\Lambda}^{\mathrm{H}}\left(\mathbf{\Lambda}\mathbf{\Lambda}^{\mathrm{H}}\sigma_{\mathrm{a}}^2 + \mathbf{I}\sigma^2\right)^{-1}\left(\mathbf{Y} - \mathbf{\Lambda}\mathbf{F}^{\mathrm{H}}\boldsymbol{\mu}_{\mathbf{d}}^{\mathrm{a}}\right) \tag{3}$$

$$\text{and} \quad \sigma_{\mathrm{p}}^2 = \lambda^{-1} - \sigma_{\mathrm{a}}^2, \tag{4}$$

respectively. In equation (3), $\boldsymbol{\mu}_{\mathbf{d}}^{\mathrm{a}}$ is the a-priori mean of the data symbols and σ_{a}^2 is the error variance which is equal for all symbols. As shown in [9], the assumption of equally a-priori symbols enables the equalization matrix division in (3) to be performed with element-wise multiplication, which considerably reduces the complexity without performance degradation.

[1]Notice that $\mathbf{F}$ has size $N \times N$, which is omitted for notational simplicity.

The normalization coefficient λ forces the symbols estimate to be unbiased [15], and it is computed as [9]

$$\lambda = \frac{1}{N}\mathrm{Tr}(\mathbf{\Lambda}^{\mathrm{H}}\left(\mathbf{\Lambda}\mathbf{\Lambda}^{\mathrm{H}}\sigma_{\mathrm{a}}^2 + \mathbf{I}\sigma^2\right)^{-1}\mathbf{\Lambda}), \tag{5}$$

where $\mathrm{Tr}(\cdot)$ returns the trace of of a matrix in its argument.

2) Extrinsic LLR: The extrinsic log-likelihood ratios (LLRs) are computed based on $\boldsymbol{\mu}_{\mathbf{d}}^{\mathrm{p}}$ and σ_{p}^2 as

$$(\mathbf{L})_{s,b}^{\mathrm{e}} = \frac{1}{\sigma_{\mathrm{p}}^2}\left(\min_{d\in\mathcal{S}_b^{(0)}}|d - (\boldsymbol{\mu}_{\mathbf{d}}^{\mathrm{p}})_s|^2 - \min_{d\in\mathcal{S}_b^{(1)}}|d - (\boldsymbol{\mu}_{\mathbf{d}}^{\mathrm{p}})_s|^2\right), \tag{6}$$

where $\mathcal{S}_b^{(0)}$ and $\mathcal{S}_b^{(1)}$ represents the sets of constellation symbols in which the bth bit is 0 or 1, respectively. Equation (6) is an approximation that assumes independence of the noise component in each symbol and neglects the a-priori knowledge of each bit. However, it is worth mentioning that a minimum impact on the performance is observed when compared with the exact LLR computation [17].

3) SISO Decoder: This block calculates the a-priori LLR of the coded bits $\mathbf{L}^{\mathrm{a}}$ based on the extrinsic LLRs as input. In this paper, we compare two types of encoder and decoders, namely, i) recursive systematic convolutional code with BCJR log-MAP decoder, and ii) quasi-cyclic LDPC (QC-LDPC) [18] with sum-product algorithm (SPA) for decoding [19]. Note that the interleaving and deinterleaving operations are performed inside the decoder block for simplicity of the diagram.

Lastly, the information bits are estimated as $\hat{b}$ by comparing the LLRs corresponding to the information bits with zero. By employing a cyclic redundancy check (CRC), the receiver halts when the information bits are correctly estimated. Otherwise, it stops when reaching the maximum number of iterations.

4) A-priori Soft Symbol: The a-priori mean and variance of $\mathbf{d}$ are computed based on the a-priori LLRs provided by the SISO decoder. Let $(\mathbf{L})_{s,b}^{\mathrm{a}}$ be the a-priori LLR of the sth data symbol at the bth bit position. Next, for the bth bit of the sth symbol $x_{s,b} \in \{0,1\}$, its probabilities of assuming 1 or 0 are given by $\Pr\{x_{s,b} = 1\} = \frac{1}{1+\exp\left((\mathbf{L})_{s,b}^{\mathrm{a}}\right)}$ and $\Pr\{x_{s,b} = 0\} = \frac{1}{1+\exp\left(-(\mathbf{L})_{s,b}^{\mathrm{a}}\right)}$, respectively. Then, the probability mass function of the sth data symbol, $d_s \in \mathcal{S}$, is given by $\Pr\{d_s = d\} = \prod_b \Pr\left\{x_{s,b} = \mathcal{X}_b(d)^{-1}\right\}$, where $\mathcal{X}_b(d)^{-1}$ is the QAM-to-bit mapping for the bth bit. The desired a-priori mean and variance of $\mathbf{d}$ are respectively computed as [17]

$$(\boldsymbol{\mu}_{\mathbf{d}}^{\mathrm{a}})_s = \sum_{d\in\mathcal{S}}\Pr\{d_s = d\}\, d, \tag{7}$$

$$\text{and} \quad (\mathbf{\Sigma}_{\mathbf{d}}^{\mathrm{a}})_{s,s} = \sum_{d\in\mathcal{S}}\Pr\{d_s = d\}\,|d - (\boldsymbol{\mu}_{\mathbf{d}}^{\mathrm{a}})_s|^2. \tag{8}$$

Since the equalizer in (3) assumes equal-reliable symbols, the a-priori error level for each symbol estimate is given by

$$\sigma_{\mathrm{a}}^2 = \frac{1}{N}\mathrm{Tr}(\mathbf{\Sigma}_{\mathbf{d}}^{\mathrm{a}}). \tag{9}$$

We highlight that in the first iteration there is no a-priori information available on the LLRs. In this case, $\mathbf{L}_{s,b}^{\mathrm{a}} = 0$ for all s and b due to equal probability assumption of the transmitted bits. This leads to $(\boldsymbol{\mu}_{\mathbf{d}}^{\mathrm{a}})_s = 0$ for all s and $\sigma_{\mathrm{a}}^2 = 1$.

This document is a preprint of: R. Bomfin, A. Nimr and G. Fettweis, "A Study on Iterative Equalization for DFTs-OFDM Waveform under sub-THz Channels," in Proceedings of 2022 IEEE 19th Annual Consumer Communications Networking Conference (CCNC 2022), Virtual Conference, (pp. 1-6), Jan 2022. DOI:10.1109/CCNC49033.2022.9700594

TABLE I
MEASUREMENTS OF [7] USED IN SECTION IV.

Channel	Tx ID	distance (m)	ϕ (°)
I	1	5.10	42
II	13	15.04	223
III	13	15.04	209

III. EMPIRICAL SUB-THZ CHANNEL MODEL

In this section the empirical $140\,\mathrm{GHz}$ sub-THz channel model is described. We utilize the measurements presented in [7], [8], which have been collected via the spatio-temporal channel sounder from Aalto University, Finland. In this paper, we use the measurements performed on the shopping mall "Sello" in Espoo, Finland, that is a modern four-story building with approximately $120 \times 70\,\mathrm{m}^2$. The measurements are performed with bandwidth of $4\,\mathrm{GHz}$ and center frequency of $143\,\mathrm{GHz}$. For transmitting the sounding signal, an omnidirectional antenna with $60°$ elevation beamwidth is utilized. At the receiver, a horn antenna is utilized with 19 dBi gain with $10°$ and $40°$ of azimuth and elevation beamwidth, respectively. Thus, by rotating the receiver horn antenna, it is possible to obtain resolved channel impulse responses in the angular domain. The references [7], [8] contain more detailed information about the measurement setup.

A. Discrete-Time Channel Model

The data considered in this work consists of PADP measurements with significant local maxima within the dynamic range. We term the PADP as $P_{\text{measured}}(\phi, \tau)$, where ϕ and τ denote the receiver antenna angle in degree and path delay in seconds, respectively. In addition, since we consider a discrete-time system in (2), we map the PADP $P_{\text{measured}}(\phi, \tau)$ into a discrete-time model as

$$\rho_{n,\phi} = h_{\text{measured}}(\phi, \tau). \tag{10}$$

Here, $n = \text{round}(\tau B)$, where B is the considered bandwidth and $\text{round}(\cdot)$ approximates its argument to the nearest integer. In order to generate random channel realizations, we follow similar approach of [20], [21], where random uniformly distributed phases are multiplied in each multi-path component. Thus, the random discrete-time channel based on the measurements of [7] is generated as

$$h_{n,\phi} = \sqrt{\rho_{n,\phi}} \exp(-j\Phi) \tag{11}$$

for a fixed receiver angle ϕ, where Φ is a random variable with uniform distribution between 0 and 2π. In the frequency domain, the random channel is given by[2]

$$\mathbf{H} = \mathbf{F}\mathbf{h}, \tag{12}$$

where $\mathbf{h} = [h_{0,\phi}, h_{1,\phi}, \cdots, h_{N-1,\phi}]^{\mathrm{T}}$. For completeness, the channel in the linear model of equation (2) has precisely the elements of (12) in its diagonal, i.e., $(\mathbf{\Lambda})_{k,k} = (\mathbf{H})_k$.

[2]The angle ϕ is omitted for simplicity.

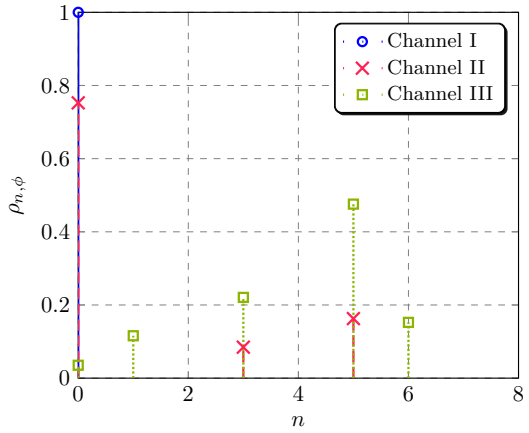

Fig. 2. Channel PDP according at the angles given in Table I.

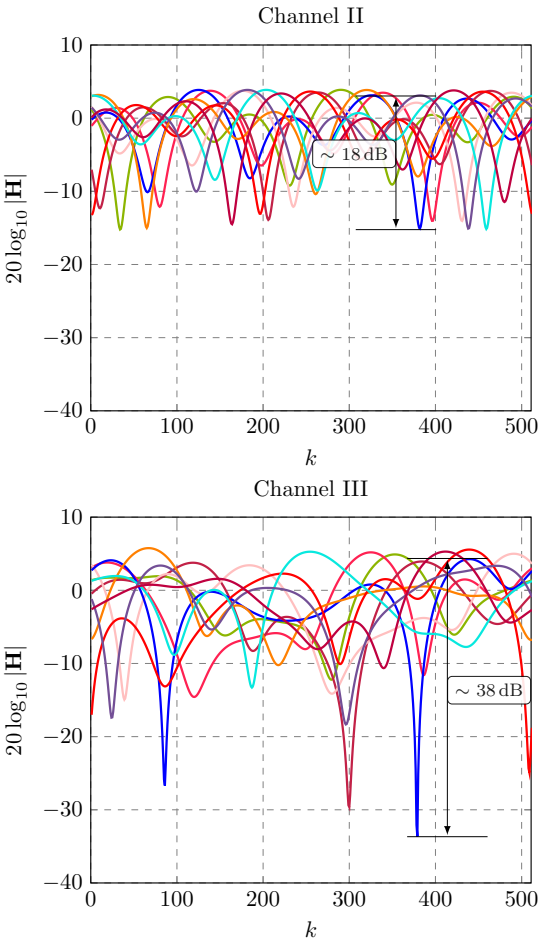

Fig. 3. Overlaid frequency-domain random channel realization gains.

B. Used Channels from [7]

In this section we analyze the channel measurements used in the numerical results of Section IV. We selected three measurement sets from [7], which are given in Table I, where the Tx ID is related to the transmitter location. We plot the PAPD (10) for these channels in Fig. 2. One observes that channel I is flat, and channels II and III have multi-path components for $n > 0$.

In order to verify the frequency selectivity of channels II and III, Fig. 3 depicts the overlaid power channel realizations

This document is a preprint of: R. Bomfin, A. Nimr and G. Fettweis, "A Study on Iterative Equalization for DFTs-OFDM Waveform under sub-THz Channels," in Proceedings of 2022 IEEE 19th Annual Consumer Communications Networking Conference (CCNC 2022), Virtual Conference, (pp. 1-6), Jan 2022. DOI:10.1109/CCNC49033.2022.9700594

TABLE II
SIMULATION PARAMETERS.

Parameter	Value
n. of symbols (FFT size), N	512
bandwidth	1 GHz
MCS	1/2 QPSK, 1/2 16QAM
	3/4 QPSK, 3/4 16QAM
conv. dec.	log-MAP BCJR
LDPC dec.	SPA w/ 15 iterations

of (11) in the frequency domain as in (12) for $N = 512$ and the bandwidth of 1 GHz. For Channel II, we observe a difference of approximately 18 dB between the sub-carriers with maximum and minimum power. For Channel III, this difference is approximately 38 dB, which is 20 dB more than Channel II, indicating more frequency selectivity.

C. Considerations

We have considered Channels I, II and III in our experiments in Section IV due to their level of selectivity shown in Fig. 3. However, there are other relevant aspects to be considered in future works. Firstly, it is desired to have a statistical channel model such that more general conclusions are possible, which can be done by considering a larger set of measurements. Secondly, Channels I, II and III have relatively low time dispersion, where the last path arrives in the 6th sample, which means that the DFTs-OFDM with frequency-domain equalization requires a small CP overhead for $N = 512$ that is used in Section IV. However, in general there are channels with much larger time dispersion, which should be considered while choosing the system numerology. Thirdly, the measurements from [7] assume an omnidirectional transmit antenna and receive antenna with beamwidth of 10°. It means that if a wider receiver antenna is considered, we can expect the channel to be even more time dispersive because reflections from more directions are collected. On the contrary, if the transmit antenna has also a narrow beam, which can be a typical case, we can expect less time dispersive channels.

IV. NUMERICAL RESULTS

This section aims at comparing the performance of convolutional and LDPC encoders in terms of frame error rate (FER) with the channel model of Section III. The parameters used in the simulations are given in Table II. We consider a system with $N = 512$ symbols and 1 GHz bandwidth. The considered modulation and coding scheme (MCS) are QPSK and 16QAM with both $1/2$ and $3/4$ coding rate. The $1/2$ code rate recursive systematic convolutional (RSC) encoder has the generating polynomial $\{133, 171\}_8$, and a higher code rate of $R = 3/4$ is obtained by puncturing 66% of the parity bits. The QC-LDPC code considered in this work utilizes the 5G NR base graphs BG_2 and BG_1 with code rates $R = 1/2$ and $R = 3/4$, respectively [14].

Fig. 4 shows the results with convolutional encoder. In order to assess the impact of having several iterations in the receiver, we show the results for iterations $I = \{0, 2, 4\}$. $I = 0$ means

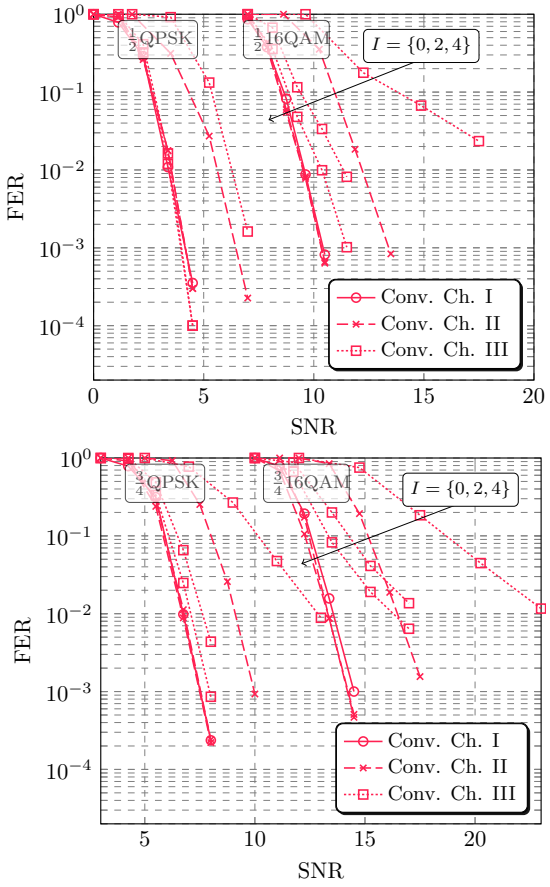

Fig. 4. FER with convolutional encoder for iterations 0, 2 and 4.

that the receiver is linear and no further interference cancellation iterations are performed. The first observation to make is that the iterative receiver considerably improves the system performance under frequency selective channels in comparison to the linear receiver, i.e., with zero iterations. For instance, for Channel II, there is an improvement of approximately 2 dB and 2.5 dB in the $1/2$ QPSK and $1/2$ 16QAM systems, respectively, when using the iterative receiver. For Channel II, one observes that 2 iterations are sufficient, since the system with 4 iterations achieves no further improvement. However, the system under Channel III, achieves further improvement with 4 iterations. This is observed in the curves of $1/2$ 16QAM, $3/4$ QPSK and $3/4$ 16QAM, where the system with 4 iterations improves the performance by approximately 1 dB in comparison to the receiver with 2 iterations. This outcome is expected since Channel III is considerably more frequency-selective than Channel II, meaning that there are higher levels of ISI, and therefore, more iterations are required.

Fig. 5 shows the results with the LDPC encoder. In general, similar conclusions to the system with convolutional can be drawn. The main differences are that i) the iterative receiver provides less performance improvement than the convolutional encoder system, and ii) the system with 2 iterations has very similar performance as the system with 4 iterations for Channel III. This indicates that the maximum number of iterations can be smaller without incurring in considerable

This document is a preprint of: R. Bomfin, A. Nimr and G. Fettweis, "A Study on Iterative Equalization for DFTs-OFDM Waveform under sub-THz Channels," in Proceedings of 2022 IEEE 19th Annual Consumer Communications Networking Conference (CCNC 2022), Virtual Conference, (pp. 1-6), Jan 2022. DOI:10.1109/CCNC49033.2022.9700594

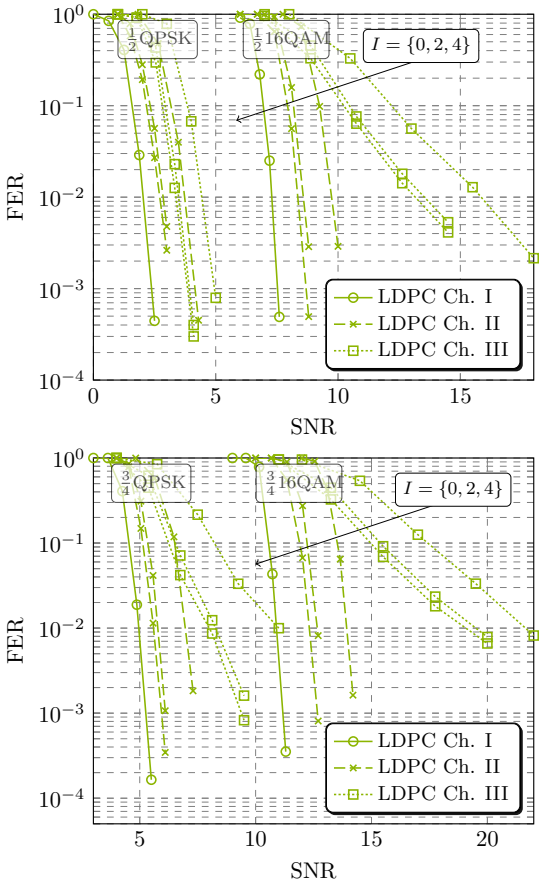

Fig. 5. FER with LDPC encoder for iterations 0, 2 and 4.

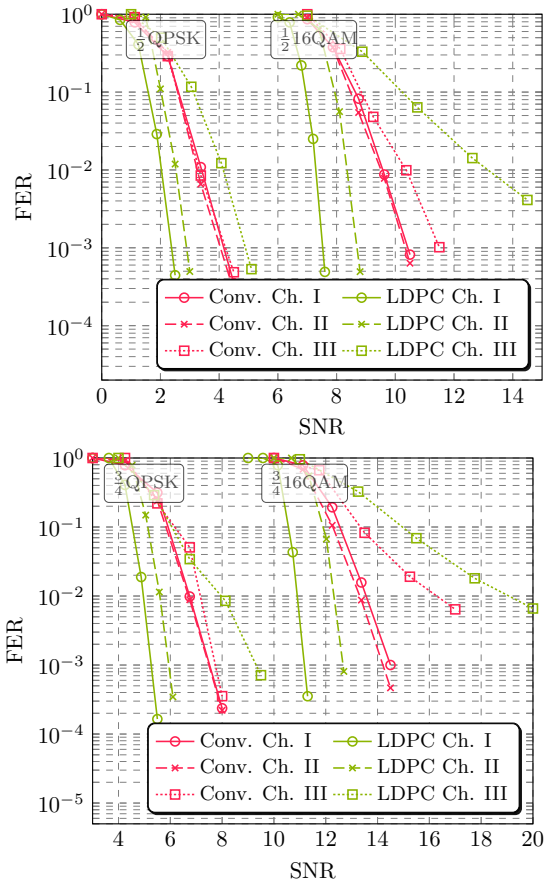

Fig. 6. FER comparison between convolutional and LDPC encoders for maximum of 4 equalization iterations.

performance loss.

In Fig. 6, we compare the system with both encoders have a maximum of 4 iterations. As expected, the system with LDPC encoder outperforms the one with convolutional for Channel I, i.e., AWGN, which has been already shown in the literature. For Channel II, the results still show that LDPC system is better, but the transmission under Channel III has a better performance with the convolutional encoder. We highlight that it is not obvious to have an exact explanation for this behavior, but it is still possible to have a general understanding of this result. First of all, although the convolutional encoder has considerably worse performance than the LDPC in the AWGN channel, we observe that it is less sensitive to the channel selectively. For instance, for the systems with $R = 1/2$, the system under Channel I has the same performance as under Channel II. In fact, for $3/4$ 16QAM, the system under Channel II is even slightly better than under Channel I. One way of explaining this is that the convolutional encoded signal, which is applied to a dispersive channel can be interpreted as a type of serially concatenated convolutional encoder. On the other hand, the system with LDPC decreases its performance as the channel becomes more selective. A similar result has already been reported in [15] under a MIMO system, where the LDPC code did not perform well under a high ISI condition. The outcomes of Fig. 6 are interesting because they inform that there is a channel selectivity level from which the convolutional code provides better performance than the LDPC code when the MMSE-PIC equalizer is employed.

Lastly, it is worth mentioning that the presented results do not lead to exact general conclusions for the sub-THz channel, because we have considered a small subset of the measured PAPD from [7]. In particular, based on our initial data analysis, the Channel III situation happens rarely, while channels resembling Channel II are more common. This observation favors the LDPC encoder choice. Therefore, more general investigation with a larger set of measurements or with statistical model is desired.

V. Conclusion and Outlook

In this work we have investigated the performance of DFTs-OFDM waveform under an empirical sub-THz channel model in 140 GHz with iterative equalization. The channel model consists of the measured PADP of [7] with uniformly distributed random phases. Since there are many occasions where the channel is frequency-selective in the measured set, we have selected three particular PADP measurements to conduct numerical link level simulations. The channels are denoted Channel I, II and III, where the first one is frequency-flat, and the renaming two are frequency-selective, being Channel II less selective than Channel III.

The outcomes of our investigation reveal that the sub-THz channel can be sufficiently frequency-selective such that

iterative equalization provides performance gain in terms of FER at the cost of extra hardware complexity in comparison to the linear one. For instance, considering Channel III (more selective), the performance gain is in the range of $1.5\,\mathrm{dB}$-$3\,\mathrm{dB}$ for the LDPC encoder, and $2\,\mathrm{dB}$-$4.5\,\mathrm{dB}$ for the convolutional encoder. Typically, higher MCS leads to a higher gain. Another interesting outcome is that the best type of encoder depends on the channel selectivity level. For instance, we have shown that for Channel I and II, the LDPC code outperforms the convolutional code, while for Channel III, the convolutional code achieves better performance than LDPC.

There are a number of possible future investigations based on this work. Firstly, a more general data set from [7] should be considered, or preferably an empirical statistical channel model, such that more general conclusions about systems at $140\,\mathrm{GHz}$ with iterative equalization can be drawn. For instance, based on our initial data analysis, it is unlikely that the Channel III represents a typical behavior at $140\,\mathrm{GHz}$, whereas situations resembling Channel II happen with higher probability. This indicates that LDPC encoder can be the best overall option. Additionally, since the LDPC decoder has internal iterations, an interesting investigation would be to decrease the number of decoding iterations while increasing the iterations of equalization. In this way, the receiver complexity would scale with the equalizer that consumes 2 FFTs per iteration without less decoding operations. Lastly, the investigation of the iterative receiver under hardware impairments, such as phase noise and power amplifier non-linearity, is of particular interest, since at higher frequencies these phenomena tend to cause major signal distortions.

ACKNOWLEDGMENTS

This work has been partly funded by the European Commission through the H2020 projects Hexa-X (Grant Agreement no. 101015956), and iNGENIOUS (Grant Agreement no. 957216). The authors would like to thank Nokia Bell-Labs and Aalto University for providing the channel measurements via the Hexa-X project. The authors would like to thank Prof. Wenjin Wang from Southeast University, China, for providing the 5G NR LDPC encoder and decoder under the joint Sino-German research project "Large-Scale and Hierarchical Bayesian Inference for Future Mobile Communication Networks".

REFERENCES

[1] M. A. Uusitalo *et al.*, "Hexa-X The European 6G flagship project," in *2021 Joint European Conference on Networks and Communications 6G Summit (EuCNC/6G Summit)*, pp. 580–585, 2021.

[2] M. A. Uusitalo *et al.*, "6G Vision, Value, Use Cases and Technologies from European 6G Flagship Project Hexa-X," *IEEE Access*, pp. 1–1, 2021.

[3] X. You *et al.*, "Towards 6G wireless communication networks: vision, enabling technologies, and new paradigm shifts," *Science China Information Sciences*, vol. 64, p. 110301, Nov 2020.

[4] G. P. Fettweis and H. Boche, "6G: The Personal Tactile Internet - And Open Questions for Information Theory," *IEEE BITS the Information Theory Magazine*, pp. 1–1, 2021.

[5] K. Rikkinen, P. Kyosti, M. E. Leinonen, M. Berg, and A. Parssinen, "THz Radio Communication: Link Budget Analysis toward 6G," *IEEE Commun. Mag.*, vol. 58, no. 11, pp. 22–27, 2020.

[6] S. B. Slimane, "Reducing the Peak-to-Average Power Ratio of OFDM Signals Through Precoding," *IEEE Transactions on Vehicular Technology*, vol. 56, no. 2, pp. 686–695, 2007.

[7] S. L. H. Nguyen, J. Järveläinen, A. Karttunen, K. Haneda, and J. Putkonen, "Comparing radio propagation channels between 28 and 140 GHz bands in a shopping mall," in *Proc. 12th European Conf. Ant. Prop. (EuCAP 2018)*, (London, UK), pp. 1–5, 2018.

[8] S. L. H. Nguyen, K. Haneda, J. Järveläinen, A. Karttunen, and J. Putkonen, "Large-scale parameters of spatio-temporal short-range indoor backhaul channels at 140 GHz," in *Proc. 2021 IEEE 93rd Veh. Tech. COnf. (VTC2021-Spring)*, (Helsinki, Finland), 2021.

[9] R. Bomfin, M. Chafii, and G. Fettweis, "Low-Complexity Iterative Receiver for Orthogonal Chirp Division Multiplexing," in *IEEE WCNC workshops*, (Marrakech, Morocco), Apr. 2019.

[10] R. Bomfin, M. Chafii, and G. Fettweis, "Performance Assessment of Orthogonal Chirp Division Multiplexing in MIMO Space Time Coding," in *2019 IEEE 2nd 5G World Forum (5GWF)*, pp. 220–225, 2019.

[11] R. Bomfin, A. Nimr, M. Chafii, and G. Fettweis, "A Robust and Low-Complexity Walsh-Hadamard Modulation for Doubly-Dispersive Channels," *IEEE Commun. Lett.*, vol. 25, no. 3, pp. 897–901, 2021.

[12] T. Zemen, M. Hofer, D. Löschenbrand, and C. Pacher, "Iterative Detection for Orthogonal Precoding in Doubly Selective Channels," in *2018 IEEE 29th Annual International Symposium on Personal, Indoor and Mobile Radio Communications (PIMRC)*, pp. 1–7, 2018.

[13] F. Long, K. Niu, C. Dong, and J. Lin, "Low Complexity Iterative LMMSE-PIC Equalizer for OTFS," in *ICC 2019 - 2019 IEEE International Conference on Communications (ICC)*, pp. 1–6, 2019.

[14] 3GPP TS 38.212, "NR; Multiplexing and channel coding (Release 15)," 2018.

[15] M. Matthé, D. Zhang, and G. Fettweis, "Low-complexity iterative mmse-pic detection for mimo-gfdm," *IEEE Trans. Commun.*, vol. 66, pp. 1467–1480, April 2018.

[16] G. Caire, G. Taricco, and E. Biglieri, "Bit-interleaved coded modulation," *IEEE Trans. Inf. Theory*, vol. 44, no. 3, pp. 927–946, 1998.

[17] C. Studer, S. Fateh, and D. Seethaler, "ASIC Implementation of Soft-Input Soft-Output MIMO Detection Using MMSE Parallel Interference Cancellation," *IEEE J. Solid-State Circuits*, vol. 46, pp. 1754–1765, July 2011.

[18] L. Zhang, Q. Huang, S. Lin, K. Abdel-Ghaffar, and I. F. Blake, "Quasi-Cyclic LDPC Codes: An Algebraic Construction, Rank Analysis, and Codes on Latin Squares," *IEEE Trans. Commun.*, vol. 58, no. 11, pp. 3126–3139, 2010.

[19] F. Kschischang, B. Frey, and H.-A. Loeliger, "Factor graphs and the sum-product algorithm," *IEEE Trans. Inf. Theory*, vol. 47, no. 2, pp. 498–519, 2001.

[20] E. N. Papasotiriou, A.-A. A. Boulogeorgos, K. Haneda, M. F. de Guzman, and A. Alexiou, "An experimentally validated fading model for THz wireless systems," *Scientific Reports*, vol. 11, p. 18717, Sep 2021.

[21] D. Selimis, K. Ntontin, F. Lazarakis, and K. Haneda, "Initial Investigation of D-band Small-Scale Fading Statistics," in *2021 15th European Conference on Antennas and Propagation (EuCAP)*, pp. 1–5, 2021.